

Constraints on the electron-to-proton mass ratio variation at the epoch of reionization

S. A. Levshakov^{1,2,3*}, M. G. Kozlov^{2,3}, I. I. Agafonova³

¹*Ioffe Physical-Technical Institute, 194021 St. Petersburg, Russia*

²*Petersburg Nuclear Physics Institute, 188300 Gatchina, Russia*

³*Electrotechnical University “LETI”, 197376 St. Petersburg, Russia*

Accepted 2020 August 25. Received 2020 August 25; in original form 2020 July 29

ABSTRACT

Far infrared fine-structure transitions of [C I] and [C II] and rotational transitions of CO are used to probe hypothetical variations of the electron-to-proton mass ratio $\mu = m_e/m_p$ at the epoch of reionization ($z > 6$). A constraint on $\Delta\mu/\mu = (\mu_{\text{obs}} - \mu_{\text{lab}})/\mu_{\text{lab}} = (0.7 \pm 1.2) \times 10^{-5}$ (1σ) obtained at $\bar{z} = 6.31$ is the most stringent up-to-date limit on the variation of μ at such high redshift. For all available estimates of $\Delta\mu/\mu$ ranging between $z = 0$ and $z \sim 1100$, – the epoch of recombination, – a regression curve $\Delta\mu/\mu = k_\mu(1+z)^p$, with $k_\mu = (1.6 \pm 0.3) \times 10^{-8}$ and $p = 2.00 \pm 0.03$, is deduced. If confirmed, this would imply a dynamical nature of dark matter/dark energy.

Key words: cosmology: observations – cosmological parameters – techniques: spectroscopic – quasars: individual: J0439+1634, J2310+1855 – elementary particles

1 INTRODUCTION

A plethora of models for the dark sector (dark matter and dark energy) suppose the existence of Higgs-like scalar field(s) which couple non-universally to the matter content of the Standard Model (SM) of particle physics (for reviews see, e.g., Battaglieri et al. 2017; Irastorza & Redondo 2018; Beacham et al. 2019). Such coupling could change the masses of particles, thus leading to violation of the weak equivalence principle, and giving rise to the so-called *5th force*. However, all attempts to discover traces of any interaction beyond the SM in experiments on Earth and even in satellite missions have led to a null result (Thompson 2019a,b, 2018, 2017; Banerjee et al. 2018; Bergé et al. 2018; Antoniou & Perivolaropoulos 2017; Rider et al. 2016; Brax & Davis 2016; Li et al. 2016; Hamilton et al. 2015; Wagner et al. 2012). This means that the *5th force* – if exists – should be extremely long-ranged (with characteristic scales of order of galactic to intergalactic distances) and/or some screening mechanisms should be present which suppress the coupling strength in the environments where the experiments were performed (Brax 2018). In this respect the objects where the non-standard interactions could be expected from either the phenomenology or from theoretical considerations are more amenable to search for hidden fields.

The rotational curve of the Milky Way (MW) shows

that the total matter (and the gravitational potential) within the solar circle is dominated by baryons with $\rho_b/\rho_{\text{DM}} \sim 10$, where ρ_b is the baryon density and ρ_{DM} is the density of dark matter (DM) (McGaugh 2018; McMillan 2017; Iocco et al. 2015; Sofue et al. 2009). Thus, the non-detection of a signal from the dark sector in objects located in the vicinity of the galactic position of the Sun is at least conceivable. On the other hand, studies of stellar dynamics revealed the regions where the gravitational potential indeed becomes DM-dominated – these are the low surface brightness dwarf galaxies or the outskirts of ‘normal’ galaxies. In the quest for the ‘dark’ signal, targets in such regions seem to be more favorable.

Extremely high-redshift objects also represent a perspective group. For instance, investigations of the ionization processes at redshift $z \sim 1100$ which are responsible for the temperature and polarization anisotropies of the cosmic microwave background (CMB) radiation (Hannestad 1999; Kaplinghat et al. 1999; Kujat & Scherrer 2000; Yoo & Scherrer 2003; Ichikawa et al. 2006; Planck Collaboration et al. 2015; Hart & Chluba 2020) show that the value of the Hubble constant H_0 correlates with the electron mass. As a consequence, an increased effective electron mass at the epoch of recombination, $m_{e,z} = (1.0190 \pm 0.0055)m_{e,0}$, leads to a shifted value of the Hubble constant $H_0 \simeq 71 \text{ km s}^{-1} \text{ Mpc}^{-1}$ as compared with that inferred from the Λ cold dark matter model (Λ CDM) calibrated by Planck CMB data $H_0 = 67.4 \pm 0.5 \text{ km s}^{-1} \text{ Mpc}^{-1}$ (Planck Collaboration

* E-mail: lev@astro.ioffe.ru

et al. 2018). This interplay between $m_{e,z}$ and H_0 may alleviate the so-called Hubble tension – the difference between the Hubble constant measured in the late Universe ($z \lesssim 1$), $H_0 = 74.03 \pm 1.42 \text{ km s}^{-1} \text{ Mpc}^{-1}$ (Riess et al. 2019) and $H_0 = 73.3 \pm 1.8 \text{ km s}^{-1} \text{ Mpc}^{-1}$ (Wong et al. 2019), and the CMB value.

Another high-redshift control point is the cosmic dawn ($z \lesssim 20$). The depth of the H I 21-cm absorption trough at $z = 14 - 21$ detected in EDGES by Bowman et al. (2018) turned out to be twice as large as predicted what required additional mechanisms to explain it. Many models consider now different types of non-gravitational interaction between dark and baryonic matter as factors which could cool the neutral gas (Barkana et al. 2018; Houston et al. 2018; Fraser et al. 2018; Safarzadeh et al. 2018; Yang W. et al. 2019; Famaey et al. 2020).

The subsequent epoch of reionization ($6 < z < 10$) is characterized by the progressive ionization of the previously neutral intergalactic medium that makes possible observations across much of the electromagnetic spectrum. This results in a variety of methods which can be devised to test theoretical models beyond the SM. In particular, in the present paper we probe the non-standard coupling in two objects at $z > 6$ by means of radio spectroscopy of atomic and molecular transitions. Note that the cosmic time interval between $z = 6$ and $z = 1100$ is about 900 Myr, i.e., less than $1/10\text{th}$ of the Hubble time, and between $z = 6$ and $z = 17$ is only 640 Myr¹.

The theoretically predicted coupling affects preferentially the electron mass, whereas the mass of the proton is determined by the strength of the strong interaction of quarks and remains less affected. Therefore, the electron-to-proton mass ratio $\mu = m_e/m_p$ can be used as a probe to search for the hidden scalar fields.

Measurements of this ratio employ a variety of atomic and molecular transitions which have a different sensitivity to small changes in μ , or in the fine structure constant $\alpha = e^2/\hbar c$, or in a combination of μ and α , $F = \alpha^2/\mu$. However, Higgs-like couplings assume that the variations of α – if any – are typically much smaller than those of μ (e.g., Yoo & Scherrer 2003), so that in the first approximation α can be considered as a constant. If relative offsets between different molecular frequencies induced by the alleged changes in μ are large enough, they can be measured by direct spectroscopic methods in optical and radio bands (Kozlov & Levshakov 2013; Ubachs 2018).

Up to now, the most accurate probes of μ were obtained in Galactic molecular clouds distributed in the MW disk where the Galactic gravitational potential is the same as in the Solar system and $\rho_b/\rho_{DM} \sim 10$. The upper limit (1σ) on the fractional change in μ , $\Delta\mu/\mu = (\mu_{\text{obs}} - \mu_{\text{lab}})/\mu_{\text{lab}}$, for the MW disk clouds was found to be $|\Delta\mu/\mu| < 0.9 \times 10^{-8}$ (Levshakov et al. 2013). Employing methanol (CH₃OH) absorption-line transitions, Kanekar et al. (2015) obtained $|\Delta\mu/\mu| < 0.6 \times 10^{-7}$ for a molecular cloud in a distant galaxy at $z = 0.89$ which is a high-redshift analogue to the MW, i.e., the total mass balance in this galaxy is probably dominated by baryonic matter. On the other hand,

for an object in the Large Magellanic Cloud located at the galactocentric distance where $\rho_b/\rho_{DM} < 1$ we deduced $\Delta\mu/\mu = (1.7 \pm 0.7) \times 10^{-7}$ (Levshakov et al. 2019). Similarly, a value of $\Delta\mu/\mu = (3.5 \pm 1.2) \times 10^{-7}$ was reported by Kanekar (2011) for a faint dwarf galaxy at $z = 0.69$ where the dark matter may prevail. However, the last two values may be affected by non evaluated systematics and require further investigations.

As for the measurements at high-redshifts, previously we estimated the value of $\Delta F/F = (F_{\text{obs}} - F_{\text{lab}})/F_{\text{lab}}$ for two distant quasars BR 1202–0725 ($z = 4.69$) and J1148+5251 ($z = 6.42$) where $|\Delta F/F| < 1.5 \times 10^{-4}$ (Levshakov et al. 2008), and for a lensed galaxy HLSJ091828.6+514223 at $z = 5.24$ where $|\Delta F/F| < 1.5 \times 10^{-5}$ (Levshakov et al. 2012). Later on, the result towards J1148+5251 was slightly improved to $|\Delta F/F| < 4 \times 10^{-5}$ (Levshakov et al. 2017).

Here we evaluate two additional limits on μ -variation using published IRAM/NOEMA spectra of the most distant gravitationally lensed quasar J0439+1634 at $z = 6.519$ (Yang J. et al. 2019; herein referred to as Y19) and new ALMA observations of the quasar J2310+1855 at $z = 6.003$ (Li et al. 2020; herein referred to as L20). Combining all points ranging between $z = 6.0$ and $z = 6.5$, we obtain the most stringent limit on μ variations at the end of the epoch of reionization.

2 DATA AND METHOD

The radial velocity offset, $\Delta V = V_{\text{rot}} - V_{\text{fs}}$, between low-lying rotational lines of carbon monoxide and atomic far infrared (FIR) fine-structure lines, being interpreted in terms of the fractional change in the quotient $F = \alpha^2/\mu$, or in the product $F = \tilde{\mu}\alpha^2$ gives (Levshakov et al. 2008):

$$\Delta V/c = \Delta F/F = 2\Delta\alpha/\alpha - \Delta\mu/\mu = \Delta z/(1 + \bar{z}), \quad (1)$$

or

$$\Delta V/c = 2\Delta\alpha/\alpha + \Delta\tilde{\mu}/\tilde{\mu} = \Delta z/(1 + \bar{z}). \quad (2)$$

Here $\tilde{\mu} = \mu^{-1}$, c is the speed of light, $\Delta z = z_{\text{rot}} - z_{\text{fs}}$ is the redshift difference between the rotational and fine-structure lines, \bar{z} is their mean redshift, and $z_{\text{rot}}, z_{\text{fs}}$ are related to the observed and laboratory frequencies, ν_{obs} and ν_{lab} , via

$$z = \nu_{\text{lab}}/\nu_{\text{obs}} - 1. \quad (3)$$

As already mentioned above, Higgs-like couplings do not change α . Therefore, in this paper we will assume that α is kept fixed. In this approximation, we have

$$\Delta F/F \approx -\Delta\mu/\mu. \quad (4)$$

Velocity offsets ΔV measured in astrophysical objects usually include also random shifts caused by the heterogeneous spatial distribution of different species which may not trace each other exactly. On the other hand, in the present case we analyze integrated emission over the whole surface of a distant galaxy which means that such random shifts are already to a great extent averaged. Nevertheless, we define ΔV as a sum of two components — ΔV_F due to F -variations, and ΔV_D due to random kinematic effects (the so-called Doppler noise):

$$\Delta V = \Delta V_F + \Delta V_D. \quad (5)$$

¹ Here we adopt a flat Λ CDM cosmology with $H_0 = 70 \text{ km s}^{-1} \text{ Mpc}^{-1}$, $\Omega_\Lambda = 0.7$, $\Omega_m = 0.3$.

The Doppler noise is supposed to be normally distributed with a zero mean and a finite variance, and the signal ΔV_F can be estimated statistically by averaging over a data sample:

$$\langle \Delta V \rangle = \langle \Delta V_F \rangle, \quad \text{Var}(\Delta V) = \text{Var}(\Delta V_F) + \text{Var}(\Delta V_D). \quad (6)$$

For a single system, the dispersion of the Doppler noise can be estimated from the comparison of the velocity offsets between spectral lines of similar species which are linked to each other by a certain physical conditions. In our case these are [C I], [C II], and CO lines. Low-lying rotational lines of carbon monoxide and FIR fine-structure lines of atomic carbon trace neutral gas which is well shielded from the ionizing radiation (Hollenbach & Tielens 1999) and, as a result, in molecular clouds their profiles are similar (Okada et al. 2019). As for [C II], its FIR fine-structure emission is usually enhanced at the edges of molecular clouds in the photodissociation regions (PDRs). However, diffuse gas from the H II regions can also contribute to some extent ($\lesssim 30\%$, e.g., Kaufman et al. 1999) to the intensity of the ‘PDR’ lines, being integrated over the surface distribution of the [C I]/[C II]/CO emitting gas of a galaxy. As a result, [C II] lines may have a slightly wider profiles than [C I] and CO lines if H II regions occupy considerable volume of the observed galaxy.

In the present paper, we analyze radial velocity offsets between the rotational lines of CO(5-4) 576.26793050(5) GHz, CO(6-5) 691.4730763(5) GHz, CO(7-6) 806.65180600(50) GHz, CO(8-7) 921.79970000(50) GHz, CO(9-8) 1036.91239300(50) GHz (Endres et al. 2016), and the FIR fine-structure lines of [C I] $^3P_2 \rightarrow ^3P_1$ 809.341970(17) GHz (Haris & Kramida 2017), and [C II] $^2P_{3/2} \rightarrow ^2P_{1/2}$ 1900.5369(13) GHz (Cooksy et al. 1986). These lines were observed in emission towards two distant quasars: J0439+1634 at $z = 6.519$ (Y19), and J2310+1855 at $z = 6.003$ (L20). Among them, only [C I], [C II], CO(6-5), CO(7-6) and CO(9-8) demonstrate simple symmetric profiles and were taken with the same spectral resolution, $\Delta_{\text{ch}} \simeq 50 \text{ km s}^{-1}$ per channel.

The emission lines of CO(6-5), CO(7-6) and [C I] were detected in a single setting with receiver 1 (3 mm) and the angular resolution of $\theta = 6.''2 \times 3.''2$. The CO(9-8) line was observed with receiver 2 (2 mm) and $\theta = 3.''1 \times 2.''4$, whereas observations of [C II] were performed with receiver 3 (1 mm) in two settings $\theta_1 = 4.''9 \times 1.''9$, and $\theta_2 = 1.''2 \times 0.''7$. In spite of different angular resolutions, all the IRAM/NOEMA detections are spatially unresolved.

However, J0439+1634 is a compact lensed quasar with a maximum image separation $\theta \sim 0.''2$ (Fan et al. 2019), and this fact may affect line profiles due to differential lensing, i.e., the lensing pattern of distant objects may cause complex velocity profiles of emission lines in the spatially unresolved images in case of different lensing magnifications of emitting regions (e.g., Rivera et al. 2019; Yang C. et al. 2019). This may modify the offset between the relative positions of spectral lines.

A combination of [C I]/[C II]/CO lines, — the so-called Fine Structure Method (FSM), — has already been used in differential measurements of the fundamental physical constants in a wide redshift range — from $z \simeq 0$ up to $z \simeq 7$ (Levshakov et al. 2008, 2010, 2012, 2017, 2019; Curran et al. 2011; Weiß et al. 2012). To note is also that the FSM

provides, at least, a factor of 30 more sensitive probe of the variability of physical constants than traditionally used UV and optical resonance lines of atoms and ions (Levshakov et al. 2008; Kozlov et al. 2008).

The accurate determination of the centroid (V_0) and the full width at half maximum (FWHM) of a spectral line is crucial for high-precision measurements. If the line profile is a Gaussian then the statistical uncertainty of centroid is given by (e.g., Landman et al. 1982):

$$\sigma_0 \simeq \frac{0.7 \Delta_{\text{ch}}}{\text{SN}} \sqrt{n}, \quad (7)$$

where Δ_{ch} is the channel width, SN — the signal-to-noise ratio, and $n = \text{FWHM}/\Delta_{\text{ch}}$ — the line width in units of channels.

Apart from the statistical uncertainty σ_0 , there are systematic errors related to instrumental effects such as LSR corrections, σ_{LSR} , and uncertainties in the rest frame frequencies, σ_{rest} . For instance, a long periodic trend in the LSR corrections due to the effect of Jupiter is $\sigma_{\text{LSR}} \simeq 12 \text{ m s}^{-1}$, and the largest uncertainty of the rest frame frequency of $\sigma_{\text{rest}} = 200 \text{ m s}^{-1}$ belongs to [C II] (Cooksy et al. 1986). Both of them is, however, much smaller than the channel width $\Delta_{\text{ch}} \simeq 50 \text{ km s}^{-1}$ of the spectral data in question. If, for a moment, we ignore these systematic errors, σ_{LSR} and σ_{rest} , then for a moderate quality data with $\text{SN} \sim 10 - 20$ and $n \sim 5 - 6$ the relative statistical error, $\delta_0 = \sigma_0/\Delta_{\text{ch}}$, is about $1/10\text{th}$ of the channel width. On the other hand, for a high quality data with $\text{SN} > 100$ the centroid limiting accuracy will be restricted by the systematic errors which for the case of the [C II]/CO pairs provides a limiting accuracy of $\sigma(\Delta F/F)_{\text{lim}} \simeq 7 \times 10^{-7}$, whereas for the [C I]/CO pairs it is $\simeq 2 \times 10^{-8}$.

Before processing, we subtracted baselines from each spectrum. The baseline was defined from the regression analysis of the mean signals from spectral intervals without emission lines and/or noise spikes. In each such interval the *rms* noise level was determined as well. Since individual *rms* uncertainties were of the same order of magnitude, their mean value was assigned to the whole spectrum.

3 RESULTS

3.1 Constraints on μ -variation at $z = 6.519$

IRAM/NOEMA spectra of J0439+1634 exhibit four rotational transitions of CO: $J = 6 \rightarrow 5, 7 \rightarrow 6, 9 \rightarrow 8$, and $10 \rightarrow 9$. We do not use the last one since it is blended with the H₂O $3_{1,2}-2_{2,1}$ emission line. The selected CO lines together with [C II] and [C I] are shown by black histograms in Fig. 1. Each individual line was fitted by a single-component Gaussian model (shown by red). The residual uncertainties are plotted by the lower black histograms. All emission line profiles are well described by the Gaussian model with the minimum values of χ^2 per degrees of freedom of about 1.

The derived model parameters are listed in Table 1. The strongest line is [C II] with a line flux $\mathcal{F}_{[\text{CII}]}$ more than 5 times exceeding the other line fluxes. It was also observed with a high signal-to-noise ratio. Since the measured redshift of $z_{[\text{CII}]} = 6.51877(11)$ is in good agreement with the previous result $z_{[\text{CII}]} = 6.5188(1)$ of Y19, we used [C II] as a reference line for the velocity scale shown in Fig. 1.

Table 1. Derived parameters of lines towards the quasar J0439+1634. ^aCalculated using rest frame frequencies of 1900.5369(13) GHz for [C II] $^2P_{3/2} - ^2P_{1/2}$ from Cooksy et al. (1986), 809.341970(17) GHz for [C I] $^3P_2 - ^3P_1$ from Haris & Kramida (2017), 691.4730763(5) GHz for CO(6-5), 806.65180600(50) GHz for CO(7-6), and 1036.9123930(50) GHz for CO(9-8) from Endres et al. (2016). Given in parentheses are statistical errors (1σ) in the last digits.

Transition	ν_{obs} (GHz)	FWHM (GHz)	FWHM (km s ⁻¹)	\mathcal{F} (Jy km s ⁻¹)	z^a
[C II]	252.7725(38)	0.249(12)	295(14)	10.96(5)	6.51877(11)
[C I]	107.6406(49)	0.090(12)	251(33)	0.54(15)	6.51893(34)
CO(6-5)	91.9682(13)	0.082(4)	267(13)	1.61(8)	6.51861(11)
CO(7-6)	107.2778(18)	0.101(5)	282(14)	1.60(8)	6.51928(13)
CO(9-8)	137.9120(34)	0.141(11)	315(24)	2.28(15)	6.51865(19)

In spite of a larger line width of [C II] than that of [C I] (FWHM = 294 km s⁻¹ vs. 251 km s⁻¹), both values match each other within the measured 1σ uncertainty intervals. As for the widths of the CO lines, they show a tendency of increasing FWHM with increasing J : the cold gas ($T_{\text{kin}} \lesssim 100$ K) tracers CO(6-5) and CO(7-6) have a compatible line width with that of [C I], whereas CO(9-8) is broader — the value of FWHM_{CO(9-8)} is shifted towards the width of FWHM_[CII]. Since at the galactic scales the observed line profiles are formed by the global velocity field, it indicates that the contribution of warm gas ($T_{\text{kin}} \sim 200$ K) to emissivity of [C II] and CO(9-8) may be essential for the quasar host galaxy J0439+1634. The observed similarity of line profiles implies that the warm and cold gas are well mixed throughout the galactic disk.

As mentioned above, the observed profile of [C II] is well fitted by a single-component Gaussian model. However, at $V \simeq -350$ km s⁻¹ in the residual uncertainties (Fig. 1) there is an excess of four channel widths which may indicate the presence of a weak blueshifted subcomponent. We note that a blueshift of 310 ± 120 km s⁻¹ between the main component of [C II] and the optical Mg II ($\lambda_0 = 2798$ Å) emission line from the near-infrared spectrum of J0439+1634 (Fan et al. 2019) was previously revealed in Y19.

The dispersion of the measured redshifts is illustrated in Fig. 2, left panel. The largest deviation from the reference point $z_{\text{[CII]}}$ is observed for CO(7-6) with the velocity offset $\Delta V = 20.3$ km s⁻¹, which is about one half of the channel size against an expected $\simeq 0.1\Delta_{\text{ch}}$, as in the case of [C I], CO(6-5), and CO(9-8). The reason for such a large velocity offset is unclear and probably due to some systematic effects because CO $J = 7 \rightarrow 6$ is an intermediate transition between $J = 6 \rightarrow 5$ and $J = 9 \rightarrow 8$, and, hence, its apparent shift cannot be explained as a result of varying physical conditions in emitting regions traced by different CO lines.

To estimate an upper limit on $\Delta\mu/\mu$, at first we average separately the redshifts of the fine structure lines [C I] and [C II], and the CO rotational transitions listed in Table 1. It gives $\langle z \rangle_{\text{fs}} = 6.51885(18)$ and $\langle z \rangle_{\text{rot}} = 6.51885(9)$. Then we calculated $\Delta\mu/\mu = (\langle z \rangle_{\text{rot}} - \langle z \rangle_{\text{fs}}) / (1 + \bar{z}) = (0.0 \pm 2.7) \times 10^{-5}$ (1σ).

3.2 Constraints on μ -variation at $z = 6.003$

Here we tighten our constraint on $\Delta\mu/\mu$ at $z = 6.519$ towards the quasar J2310+1855 at $z = 6.003$ using the updated values of velocity offsets between four high- J ro-

tational transitions of CO ($J = 5 \rightarrow 4$, $J = 6 \rightarrow 5$, $J = 8 \rightarrow 7$, and $J = 9 \rightarrow 8$) and the fine-structure line of [C II] $^2P_{3/2} \rightarrow ^2P_{1/2}$.

In our previous analysis of this quasar (Levshakov et al. 2017), we used the CO(6-5) line from PdBI observations with angular resolution $\theta = 5''.4 \times 3''.9$, and the [C II] line from ALMA observations with $\theta = 0''.72 \times 0''.51$ (Wang et al. 2013). The redshift of $z_{\text{CO(6-5)}} = 6.0025(7)$ and $z_{\text{[CII]}} = 6.0031(2)$ gave an upper limit on $|\Delta\mu/\mu| < 10^{-4}$. Additional observations of J2310+1855 in CO lines with ALMA (L20; Feruglio et al. 2018) and IRAM/NOEMA (L20) allow us to set a more stringent limit on $\Delta\mu/\mu$.

The detected molecular lines are listed in Table 2 of L20. Carbon monoxide emission was observed in rotational transitions from $J = 2 \rightarrow 1$ up to $J = 13 \rightarrow 12$. From this dataset we selected CO lines obtained with the highest angular resolution and with redshifts measured with errors $\sigma_z \leq 0.0004$ (Table 2). The reported line widths are distributed around the mean $\langle \text{FWHM} \rangle_{\text{CO}} = 392$ km s⁻¹ with standard deviation $\sigma_{\text{FWHM}} = 25$ km s⁻¹. The width of [C II] is in good agreement with CO lines, i.e., they all are, most probably, co-spatially distributed.

The measured redshifts with their 1σ error bars are shown in Fig. 2, right panel. Averaging five CO redshifts from Table 2 gives $\langle z \rangle_{\text{rot}} = 6.00294(13)$. With $z_{\text{fs}} = z_{\text{[CII]}} = 6.0031(2)$ the updated result at $z = 6.003$ yields $\Delta\mu/\mu = (2.3 \pm 3.4) \times 10^{-5}$ (1σ).

4 POSSIBLE Z -DEPENDENCE OF μ

If we assume that the result of Hart & Chluba (2020), $m_{e,z} = (1.0190 \pm 0.0055)m_{e,0}$, is real at the recombination epoch, then in combination with constraints on $\Delta\mu/\mu$ at lower redshifts, $z < 7$, this implies that there should be a redshift dependence of non-standard scalar field(s) coupled to ordinary matter. All available measurements of $\Delta\mu/\mu$ from the range $z \in [0, 1100]$ are plotted by dots with error bars in Fig. 3, while the detailed information on individual data points is given in Appendix. Two inserts with expanded Y -scales are used to make the error bars visible in the indicated redshift intervals.

To approximate the z -dependence of μ we employ a simple power law

$$\frac{\Delta\mu}{\mu} = k_{\mu}(1+z)^p, \quad (8)$$

Table 2. Selected parameters of lines towards J2310+1855 (Li et al. 2020). References: ¹Wang et al. 2013; ²Li et al. 2020; ³Feruglio et al. 2018. Given in parentheses are statistical errors (1σ) in the last digits.

Transition	z	FWHM (km s ⁻¹)	Δ_{ch} (km s ⁻¹)	θ (arcsec)	Facilities
[C II]	6.0031(2)	393(21)	18	0.72×0.51	ALMA ¹
CO(5-4)	6.0030(4)	409(44)	60	1.67×1.37	NOEMA ²
CO(6-5)	6.0028(3)	361(9)	23.7	0.6×0.4	ALMA ³
CO(6-5)	6.0030(3)	422(20)	60	1.42×1.19	NOEMA ²
CO(8-7)	6.0028(1)	390(15)	36	0.79×0.75	ALMA ²
CO(9-8)	6.0031(2)	376(18)	32	0.77×0.63	ALMA ²

with k_μ and p being the model parameters. A similar form was used in Hart & Chluba (2018, 2020).

The regression analysis yields $k_\mu = (1.6 \pm 0.3) \times 10^{-8}$ and $p = 2.00 \pm 0.03$ (1σ) with the corresponding regression curve shown by red in Fig. 3. We note that the null result for the power index p reported by Hart & Chluba (2020), $p = (0.7 \pm 3.1) \times 10^{-3}$, is due to the fact that their calculations were restricted by the epoch of recombination only, $\Delta z \simeq 200$ at $z = 1100$.

We also tried an exponential function depending on two parameters k'_μ and p' :

$$\frac{\Delta\mu}{\mu} = k'_\mu \exp(p'z). \quad (9)$$

The corresponding curve for $k'_\mu = 1.7 \times 10^{-8}$ and $p' = 0.013$ is shown by the dashed grey curve in Fig. 3. It is clearly seen that the points available do not allow to decide between the power law and exponential functions. However, both of them lead to a positive coefficient k_μ (k'_μ) at $z \rightarrow 0$ if the effective electron rest mass at the epoch of recombination differs from its terrestrial value.

The question arises how the obtained redshift dependence of $\Delta\mu/\mu$ with $k_\mu > 0$ can be verified?

It is obvious that the recombination point, which is crucial for the present analysis, should be confirmed in further studies of the cosmic microwave background anisotropies. We note that the fractional changes in m_e of ~ 1 -2% do not contradict the results of primordial nucleosynthesis ($z \sim 10^8$) which show that abundances of the light nuclei are not sensitive to the changes in m_e within $\pm 10\%$ (e.g., Coc et al. 2007; Uzan 2011).

At $z \sim 17$, the central redshift of the observed H I 21-cm absorption, the expected value of $\Delta\mu/\mu$ is 5×10^{-6} [Eq. (8)] or 2×10^{-8} [Eq. (9)]. Measurements at such level of sensitivity can be provided solely by radio spectroscopy of molecular and atomic transitions. However, presently neither molecular nor atomic transitions have been detected above $z \sim 10$ albeit galaxies with redshifts $z > 10$ are expected to be observed with the Atacama Large Millimeter/submillimeter Array (de Blok et al. 2016) and the James Webb Space Telescope (Behroozi et al. 2020).

For the epoch of reionization ($6 < z < 10$) the expected value of $\Delta\mu/\mu$ is less than 10^{-6} . To date, the best estimate of the fractional changes in μ at $z > 6$ is $|\Delta\mu/\mu| < 10^{-5}$, i.e., the measurement accuracy should be improved by an order of magnitude. According to Eq. (7), this level can be achieved if the exposure time will be increased by ~ 100 times at the fixed values of the channel width $\Delta_{\text{ch}} \simeq 50$ km s⁻¹ and the line width FWHM $\simeq 200$ km s⁻¹. With the

existing observing facilities this seems to be problematic if one deals with [C I]/[C II]/CO transitions.

Another way to reach an accuracy $\sim 10^{-6}$ is to use spectral lines with higher sensitivity coefficients, Q_μ , to changes in μ [see Eq. (A1) in Appendix]. For instance, the $1_1 - 2_2E$ transition of the methanol isotopologue ¹²CD₃¹⁶OH at a rest frequency of $\nu \approx 1.2$ GHz has $Q_\mu = -330$ (Jansen et al. 2011), the sensitivity coefficients of the Λ -doublet hyperfine components of the ² $\Pi_{1/2}J = 9/2$ state of OH from the interval $\Delta\nu = 89 - 193$ MHz are ranging between $Q_\mu = 212$ and 460 (Kozlov 2009). The sensitivities of these transitions to variations in μ are more than two orders of magnitude larger than $Q_\mu = 1$ used in the current studies with [C I]/CO and [C II]/CO pairs. These and other high sensitivity molecular transitions are planned to be observed with the Five-hundred-meter Aperture Spherical radio Telescope (Chen et al. 2019).

Observations of local objects ($z \sim 0$) have an important specificity that their angular sizes are larger than the aperture of a telescope. This makes possible the scanning of the local objects across their surfaces. Then spatial fluctuations of μ can be expected if some screening mechanism predicted in a number of theories is indeed at play. The currently available data show that the upper limit on the amplitude of such fluctuations is $k_\mu \lesssim 10^{-8}$. Thus, to detect the signal the spectral line positions should be measured with uncertainties of less or about 0.01 km s⁻¹. Such an accuracy can already be achieved at the existing observing facilities.

5 SUMMARY

Our main results are as follows:

- Using a combination of the [C I] and [C II] fine structure lines together with CO(6-5), (7-6), and (9-8) rotational transitions observed towards the quasar J0439+1634 by Yang J. et al. (2019), we set a limit on $\Delta\mu/\mu = (0.0 \pm 2.7) \times 10^{-5}$ at $z = 6.519$.
- A combination of the [C II] fine structure line with CO(5-4), (6-5), (8-7), and (9-8) rotational transitions from the spectrum of J2310+1855 (Li et al. 2020) yields $\Delta\mu/\mu = (2.3 \pm 3.4) \times 10^{-5}$ at $z = 6.003$.
- Two values of $\Delta\mu/\mu$ at $z = 6.519$ and $z = 6.003$, being combined with $\Delta\mu/\mu = (-1.3 \pm 7.9) \times 10^{-5}$ at $z = 6.419$ towards the quasar J1148+5251 (Levshakov et al. 2017), give a mean value of $\langle \Delta\mu/\mu \rangle = (0.7 \pm 1.2) \times 10^{-5}$ at $\bar{z} = 6.3$ which is the most stringent up-to-date limit on the fractional changes in μ at the epoch of reionization.

• Exploiting the value of $m_{e,z} = (1.0190 \pm 0.0055)m_{e,0}$ at $z = 1100$ from Hart & Chluba (2020) and all available data on $\Delta\mu/\mu$, we obtain a functional z -dependence of μ in the form $\Delta\mu/\mu = k_\mu(1+z)^p$ with $k_\mu = (1.6 \pm 0.3) \times 10^{-8}$ and $p = 2.00 \pm 0.03$. Possible ways to verify this dependence by further observations are discussed.

ACKNOWLEDGMENTS

We would like to thank our referee Wim Ubachs for useful comments and suggestions. This work was supported by the Russian Science Foundation under grant No. 19-12-00157.

DATA AVAILABILITY

Based on the published spectra obtained at the IRAM NOEMA Interferometer (project S18DO and W18EI) and at the ALMA Interferometer (project ADS/JAO.ALMA 2015.1.01265.S).

IRAM is supported by INSU/CNRS (France), MPG (Germany), and IGN (Spain). The National Radio Astronomy Observatory is a facility of the National Science Foundation operated under cooperative agreement by Associated Universities, Inc.

ALMA is a partnership of ESO, NSF (USA) and NINS (Japan), together with NRC (Canada), MOST and ASIAA (Taiwan), and KASI (Republic of Korea), in cooperation with the Republic of Chile.

Spectral data used in this study are publicly available from the corresponding papers cited herein.

REFERENCES

Antoniou I., Perivolaropoulos L., 2017, *PhRvD*, 96, 1040002
 Banerjee D., Burtsev V. E., Chumakov A. G., Cooke D., Crivelli P., Depero E., Dermenev A. V., et al., 2018, *PhRvL*, 120, 231802
 Barkana R., Outmezguine N. J., Redigol D., Volansky T., 2018, *Phs. Rev. D*, 98, 103005
 Battaglieri M., Belloni A., Chou A., Cushman P., Echenard B., Essig R., Estrada J. et al., 2017, arXiv:1707.04591 [hep-ph]
 Beacham J., Burrage C., Curtin D., De Roeck A., Evans J., Feng J.L., Gatto C., et al., 2019, arXiv:1901.09966 [hep-ex]
 Behroozi P., Conroy C., Wechsler R. H., Hearin A., Williams C. C., Moster B.P., Yung L. Y. A., et al., 2020, arXiv:2007.04988 [astro-ph.CO]
 Bergé J., Brax P., Métris G., Pernot-Borràs M., Touboul P., Uzan J.-P., 2018, *PhRvL*, 120, 141101
 Brax P., 2018, *RPPh*, 81, 016902
 Brax P., Davis A.-C., 2016, *PhRvD*, 94, 104069
 Bowman J. D., Rogers A. E. E., Monsalve R. A., Mozdzen T. J., Mahesh N., 2018, *Nature*, 555, 67
 Chen X., Ellingsen S. P., Mei Y., 2019, *RAA*, 19, 018
 Coc A., Nunes N. J., Olive K. A., Uzan J.-P., Vangioni E., 2007, *PhRvD*, 76, 023511
 Cooky A. L., Blake G. A., Saykally R. J., 1986, *ApJL*, 305, L89
 Curran S. J., Tanna A., Koch F. E., Berengut J. C., Webb J. K., Stark A. A., Flambaum V. V., 2011, *A&A*, 533, A55
 Daprà M., Henkel C., Levshakov S. A., Menten K. M., Müller S., Bethlehem H. L., Ubachs W., 2017, *MNRAS*, 472, 4434
 de Blok W. J. G., Walter F., Smith J.-D. T., Herrera-Camus R., Bolatto A. D., Requena-Torres M. A., Crocker A. F., et al., 2016, *AJ*, 152, 51

Endres C. P., Schlemmer S., Schilke P., Stutzki J., Müller H. S. P., 2016, *J. Mol. Spectrosc.*, 327, 95
 Famaey B., Khoury J., Penco R., Sharma A., 2020, *JCAP*, 06, 025
 Fan X., Wang F., Yang J., Keeton C. R., Yue M., Zabludoff A., Bian F., et al., 2019, *ApJ*, 870, L11
 Flambaum V. V., Kozlov M. G., 2007, *PhRvL*, 98, 240801
 Fraser S., Hektor A., Hütsi G., Kannike K., Marzo C., Marzola L., Racioppi A., et al., 2018, *Phys. Lett. B*, 785, 159
 Hamilton P., Jaffe M., Haslinger P., Simmons Q., Müller H., Khoury J., 2015, *Science*, 349, 849
 Hannestad S., 1999, *PhRvD*, 60, 023515
 Haris K., Kramida A., 2017, *ApJS*, 233, 16
 Hart L., Chluba J., 2020, *MNRAS*, 493, 3255
 Hart L., Chluba J., 2018, *MNRAS*, 474, 1850
 Hollenbach D. J., Tielens A. G. G., 1999, *Rev. Mod. Phys.*, 71, 173
 Houston N., Li C., Li T., Yang Q., Zhang X., 2018, *PhRvL*, 121, 111301
 Ichikawa K., Kanzaki T., Kawasaki M., 2006, *PhRvD*, 74, 023515
 Iocco, F., Pato M., Bertone G., 2015, *NPhys.*, 11, 245-248
 Irastorza I.G., Redondo J., 2018, *PrPNP*, 102, 89
 Jansen P., Xu L. H., Kleiner I., Ubachs W., Bethlehem H. L., 2011, *PhRvL*, 106, 100801
 Kanekar N., 2011, *ApJ*, 728, L12
 Kanekar N., Ghosh T., Chengalur J. N., 2018, *PhRvL*, 120, 061302
 Kanekar N., Ubachs W., Menten K. M., Bagdonaite J., Brunthaler A., Henkel C., Müller S., et al., 2015, *MNRAS*, 448, L104
 Kanekar N., Langstone G. I., Stocke J. T., Carilli L. C., Menten K. L., 2012, *ApJ*, 746, L16
 Kanekar N., Prochaska J. X., Ellison S. L., Chengalur J. N., 2010, *ApJ*, 712, L148
 Kaplinghat M., Scherrer R. J., Turner M. S., 1999, *PhRvD*, 60, 023516
 Kaufman M. J., Wolfire M. G., Hollenbach D. J., Luhman M. C., 1999, *ApJ*, 527, 795
 Kozlov M. G., 2009, *PhRvA*, 80, 022118
 Kozlov M. G., Levshakov S. A., 2013, *Ann. Phys.* 525, 452
 Kozlov M. G., Porsev S. G., Levshakov S. A., Reimers D., Molaro P., 2008, *PhRvA*, 77, 032119
 Kujat J., Scherrer R. J., 2000, *PhRvD*, 62, 023510
 Landman D. A., Roussel-Dupré R., Tanigawa G., 1982, *ApJ*, 261, 732
 Levshakov S. A., Ng K.-W., Henkel C., Mookerjea B., Agafonova I. I., Liu S.-Y., Wang W.-H., 2019, *MNRAS*, 487, 5175
 Levshakov S. A., Ng K.-W., Henkel C., Mookerjea B., 2017, *MNRAS*, 471, 2143
 Levshakov S. A., Reimers D., Henkel C., Winkel B., Mignano A., Centurión M., Molaro P., 2013, *A&A*, 559, A91
 Levshakov S. A., Combes F., Boone F., Agafonova I. I., Reimers D., Kozlov M. G., 2012, *A&A*, 540, L9
 Levshakov S. A., Molaro P., Reimers D., 2010, *A&A*, 516, A113
 Levshakov S. A., Reimers D., Kozlov M. G., Porsev S. G., Molaro P., 2008, *A&A*, 479, 719
 Li J., Wang R., Riechers D., Walter F., Decarli R., Venamans B. P., Neri R., et al., 2020, *ApJ*, 2020, 889, 162 [L20]
 Li K., Arif M., Cory D. G., Haun R., Heacock B., Huber M. G., Nsofini J., et al., 2016, *PhRvD*, 93, 062001
 McGaugh S. S., 2018, *RNAAS*, 2, 37
 McMillan P. J., 2017, *MNRAS*, 465, 76
 Okada Y., Güsten R., Requena-Torres M. A., Röllig M., Stutzki J., Graf U. U., Hughes A., 2019, *A&A*, 621, A62
 Planck Collaboration et al., 2018, arXiv:1807.06209 [astro-ph.CO]
 Planck Collaboration et al., 2015, *A&A*, 580, A22
 Rider A. D., Moore D. C., Blakemore C. P., Louis M., Lu M., Gratta G., 2016, *PhRvL*, 117, 101101

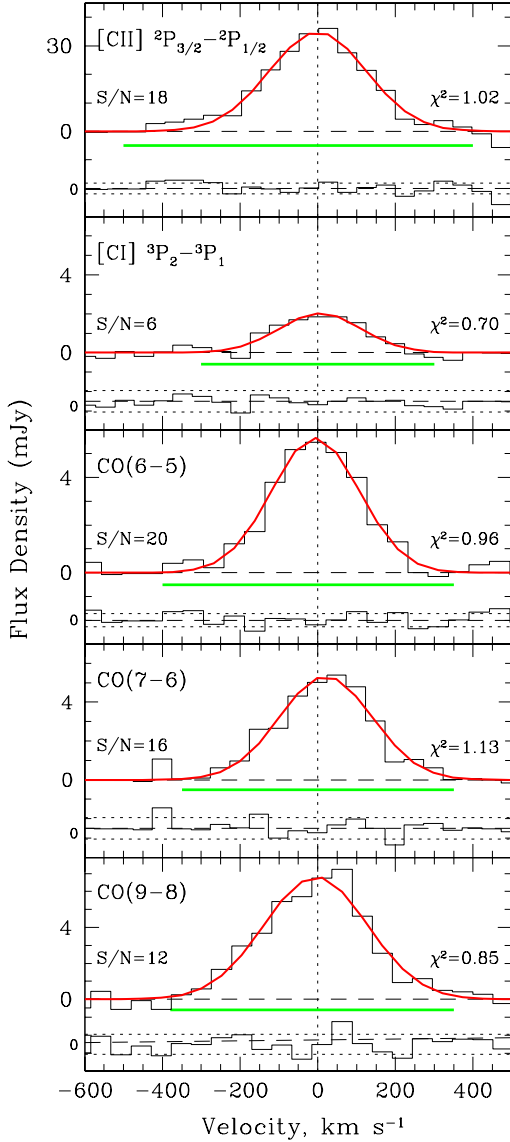


Figure 1. Black histograms are the baseline subtracted emission lines detected by Yang J. et al. (2019) towards the quasar J0439+1634. The velocity axis is relative to the redshift of [C II] given in Table 1. The red continuous lines show the model profiles. The horizontal green bars specify the velocity range used in the line fitting procedure. The residuals are plotted by the lower black histogram (arbitrarily offset for clarity). Two horizontal dotted lines are the mean $\pm 1\sigma$ noise level. The vertical dotted line marks the [C II] centroid given to indicate small velocity offsets for other emission lines. The signal-to-noise ratio (S/N) per bin at the line peak is depicted in each panel.

Riess A. G., Casertano S., Yuan W., Macri L. M., Scolnic D., 2019, *ApJ*, 876, 85
 Rivera J., Baker A. J., Gallardo P. A., Megan B., Harris A. I., Haffenberger K. M., Hughes J. P., et al., 2019, *ApJ*, 879, 95
 Safarzadeh M., Scannapieco E., Babul A., 2018, *ApJ*, 859, L18
 Sofue Y., Honma M., Omodaka T., 2009, *PASJ*, 61, 227
 Thompson R., 2019a, *MNRAS*, 490, 2019
 Thompson R., 2019b, *MNRAS*, 482, 5448
 Thompson R., 2018, *MNRAS*, 477, 4104
 Thompson R., 2017, *MNRAS*, 467, 4558

Ubachs W., 2018, *Space Sci. Rev.*, 214, 3
 Ubachs W., Salumbides E. J., Murphy M. T., Abgrall H., Roueff E., 2019, *A&A*, 622, A127
 Ubachs W., Bagdonaite J., Salumbides E. J., Murphy M. T., Kaper L., 2016, *Rev. Mod. Phys.*, 88, 021003
 Wagner T. A., Schlamming S., Gundlach J. H., Adelberger E. G., 2012, *Class. Quantum Grav.*, 29, 184002
 Wang R., Wagg J., Carilli C. L., Walter F., Lentati L., Fan X., Riechers D. A., Bertoldi F., et al., 2013, *ApJ*, 773, 44
 Weiß A., Walter F., Downes D., Carilli C. L., Henkel C., Menten

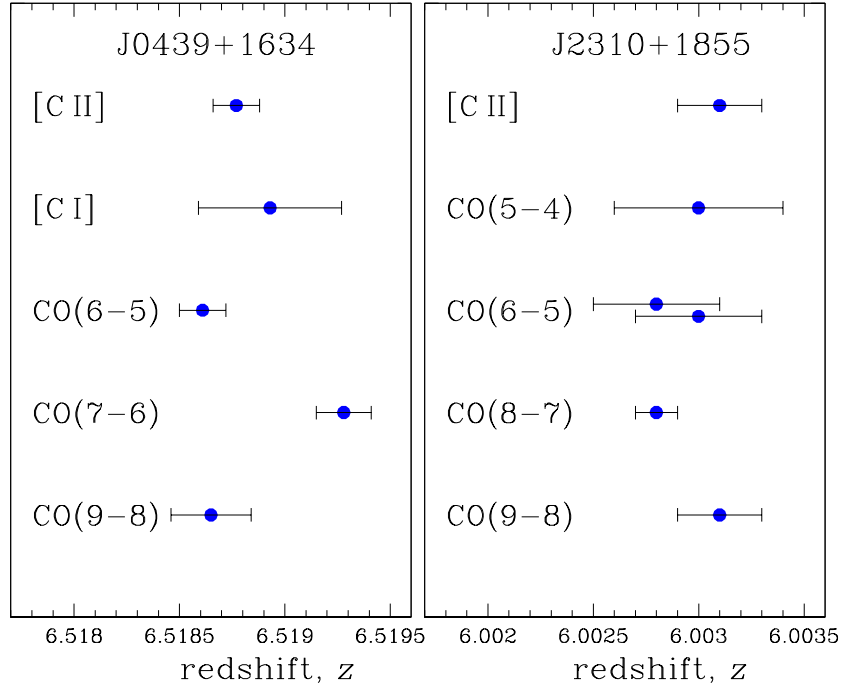


Figure 2. Measured redshifts of spectral lines towards J0439+1634 and J2310+1855 and their 1σ statistical errors listed in Table 1 and 2, respectively. The two observations of CO(6-5) towards J2310+1855 were obtained at different telescopes which are indicated in Table 2.

K. M., Cox P., 2012, ApJ, 753, 102
Wong K., Suyu S. H., Chen G. C.-F., Rusu C. E., Millon M., Sluse D., Bonvin V., et al., 2019, arXiv:1907:04869 [astro-ph.CO]
Yang C., Gavazzi R., Beelen A., Cox P., Omont A., Lehnert M. D., Gao Y., et al., 2019, A&A, 624, A138
Yang J., Venemans B., Wang F., Fan X., Novak M., Decarli R., Walter F., et al., 2019, ApJ, 880, 153 [Y19]
Yang W., Pan S., Vagnozzi S., Di Valentino E., Mota D. F., Capozziello S., 2019, JCAP, 11, 044
Yoo K. J., Scherrer R. J., 2003, PhRvD, 67, 043517

APPENDIX A: DESCRIPTION OF THE DATA POINTS

The data points shown in Fig. 3 were compiled from the following sources.

Milky Way disk ($z = 0$). In the Milky Way, high-resolution spectral observations of dark clouds were performed in the inversion line of $\text{NH}_3(1,1)$ and pure rotational lines of other molecules (the so-called ammonia method) at the Medicina 32-m and the Effelsberg 100-m radio telescopes to measure

the radial velocity offset, $\Delta V = V_{\text{rot}} - V_{\text{inv}}$, between the rotational and inversion transitions to calculate

$$\frac{\Delta\mu}{\mu} = \frac{V_{\text{rot}} - V_{\text{inv}}}{c(Q_{\text{inv}} - Q_{\text{rot}})} \approx 0.3 \frac{\Delta V}{c}, \quad (\text{A1})$$

where c is the speed of light, and $Q_{\text{inv}}, Q_{\text{rot}}$ are the corresponding sensitivity coefficients to changes in μ (Flambaum & Kozlov 2007).

In Effelsberg observations, 19 independent offsets of ΔV gave a weighted mean $\langle \Delta V \rangle = 0.003 \pm 0.006 \text{ km s}^{-1}$ (1σ) which constrained the μ -variation at the level of $\Delta\mu/\mu = (0.3 \pm 0.6) \times 10^{-8}$. The Medicina observations of two dark clouds L1521 and L1498 provided respectively $\Delta\mu/\mu = (0.1 \pm 2.2) \times 10^{-8}$ and $\Delta\mu/\mu = (-0.1 \pm 2.3) \times 10^{-8}$ (Levshakov et al. 2013).

Later on, the dark cloud core L1498 was observed with the IRAM 30-m telescope in methanol CH_3OH lines (Daprà et al. 2017), which resulted in $\Delta\tilde{\mu}/\tilde{\mu} = (-3.3 \pm 1.9) \times 10^{-8}$ or $\Delta\mu/\mu = (3.3 \pm 1.9) \times 10^{-8}$. Thus, a combined Medicina and IRAM limit on $\Delta\mu/\mu$ towards L1498 is $\Delta\mu/\mu = (3.2 \pm 1.5) \times 10^{-8}$. Now, if we add this value to both the Medicina L1521 and Effelsberg 19 clouds measurements,

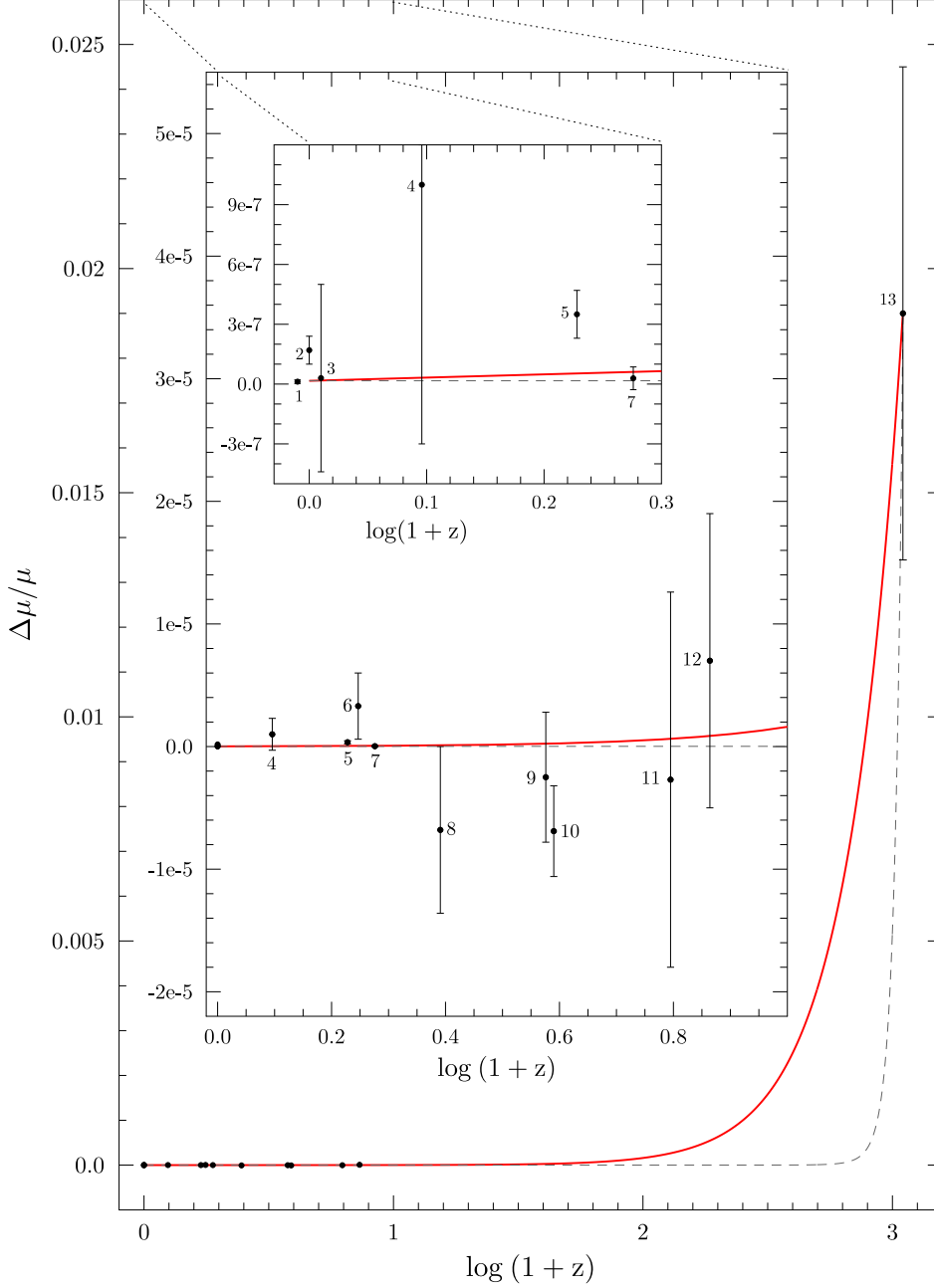


Figure 3. Constraints on the fractional changes in μ (dots with 1σ error bars) as a function of redshift z in units of $\log_{10}(1+z)$. Point 13 represents the fractional change in the rest electron mass $m_{e,0}$ at the epoch of recombination ($z \sim 1100$). Two inserts zoom consequently the corresponding parts of the data sample using different horizontal and vertical scales. Points 1, 2, and 3 at $z = 0$ are slightly shifted with respect to each other in order to resolve blending. Shown by red is a two-parameter regression curve $\Delta\mu/\mu = k_\mu(1+z)^p$ with $k_\mu = (1.6 \pm 0.3) \times 10^{-8}$ and $p = 2.00 \pm 0.03$ (1σ). The dashed grey curve is an exponential function $\Delta\mu/\mu = k'_\mu \exp(p'z)$ with $k'_\mu = 1.7 \times 10^{-8}$ and $p' = 0.013$. References for data points: 1 – Levshakov et al. (2013); 2 – Levshakov et al. (2019); 3 – Levshakov et al. (2017); 4 – Kanekar et al. (2018); 5 – Kanekar (2011); 6 – Kanekar et al. (2012); 7 – Kanekar et al. (2015); 8 – Kanekar et al. (2010); 9 – Ubachs et al. (2016, 2019); 10 – Wieß et al. (2012); 11 – Levshakov et al. (2012); 12 – this work; 13 – Hart & Chluba (2020).

then the mean constraint on $\Delta\mu/\mu$ in the MW disk reads $\langle\Delta\mu/\mu\rangle = (1.2 \pm 0.9) \times 10^{-8}$ (1σ).

Magellanic Clouds ($z = 0$). Analyzing data of 9 molecular clouds in the Large and Small Magellanic Clouds, we obtained for a highest resolution spectrum of a target PDR3-NE (LMC) an offset $\Delta V = -0.05 \pm 0.02$ km s $^{-1}$ between the CO(7-6) and [C I] lines (Levshakov et al., 2019). Being interpreted in terms of α^2/μ variations, this gives $\Delta F/F = (-1.7 \pm 0.7) \times 10^{-7}$, or $\Delta\mu/\mu = (1.7 \pm 0.7) \times 10^{-7}$ (1σ) if we assume that $|\Delta\alpha/\alpha| \ll |\Delta\mu/\mu|$.

Triangulum galaxy M33 ($z \approx 0$). 46 emitters in the CO(2-1) and [C II] lines towards M33 show an offset $\langle\Delta V\rangle = -0.01 \pm 0.14$ km s $^{-1}$ (Levshakov et al. 2017), which corresponds to $\langle\Delta F/F\rangle = (-0.3 \pm 4.7) \times 10^{-7}$, or $\langle\Delta\mu/\mu\rangle = (0.3 \pm 4.7) \times 10^{-7}$ (1σ).

Quasar PKS 1413+135 ($z = 0.25$). The conjugate satellite OH 18 cm lines at redshift $z = 0.247$ observed in emission (1720 MHz line) and absorption (1612 MHz) towards the BL Lacertae-type quasar PKS 1413+135 yield $\Delta\tilde{\mu}/\tilde{\mu} = (-1.0 \pm 1.3) \times 10^{-6}$ (Kanekar et al. 2018), or $\Delta\mu/\mu = (1.0 \pm 1.3) \times 10^{-6}$ (1σ).

Gravitational lens system B0218+357 ($z = 0.69$). The ammonia method was applied to the inversion (NH $_3$) and rotational (CS, H $_2$ CO) absorption lines detected in a lensed galaxy at $z = 0.69$ towards B0218+357 (Kanekar 2011). The measured fractional changes in μ are limited at the level of $\Delta\mu/\mu = (3.5 \pm 1.2) \times 10^{-7}$ (1σ).

Quasar J0134–0931 ($z = 0.765$). A comparison between H I 21-cm and OH 18-cm absorption lines sets a limit on $\Delta X/X = (-5.2 \pm 4.3) \times 10^{-6}$, where $X = g_p(\tilde{\mu}\alpha^2)^{1.57}$ and g_p is the proton g-factor (Kanekar et al. 2012). Assuming that fractional changes in g_p and α are smaller than those in μ , we obtain $\Delta\mu/\mu = (3.3 \pm 2.7) \times 10^{-6}$ where error includes both the statistical and systematic uncertainties.

Gravitational lens system PKS1830–211 ($z = 0.89$). In Kanekar et al. (2015), the $z = 0.89$ gravitational lens towards PKS1830–211 was observed in methanol CH $_3$ OH absorption lines yielding $\Delta\mu/\mu = (0.29 \pm 0.57) \times 10^{-7}$ (1σ).

Quasars Q 2337–011 ($z = 1.36$) and **Q 0458–020** ($z = 1.56$). Two absorbers at $z = 1.36$ and $z = 1.56$ towards respectively Q 2337–011 and Q 0458–020 were studied in the H I 21-cm and C I $\lambda\lambda 1560, 1657$ Å lines to set constraints on the product $X = g_p\tilde{\mu}\alpha^2$, where g_p is the proton g-factor (Kanekar et al. 2010). The mean value of $\Delta X/X = (6.8 \pm 1.0_{\text{stat}} \pm 6.7_{\text{sys}}) \times 10^{-6}$ transforms to $\Delta\mu/\mu = (-6.8 \pm 6.8) \times 10^{-6}$ at $\bar{z} = 1.46$ if we assume that fractional changes in g_p and α are smaller than those in μ .

H $_2$ absorption-line systems ($\bar{z} = 2.76$). In the interval from $z = 2.05$ to $z = 4.22$, the μ -variation can be constrained from a sample of nine H $_2$ systems selected from Ubachs et al. (2016, 2019). We list these measurements of $\Delta\mu/\mu$ along with their weighted mean value in Table A1. At the mean redshift $\bar{z} = 2.763$, one finds $\langle\Delta\mu/\mu\rangle = (-2.5 \pm 5.3) \times 10^{-6}$.

QSO host galaxy RXJ0911.4+0551 ($z = 2.79$). One of the most attractive target for high-precision $\Delta F/F$ measurements is the quasar host galaxy RXJ0911.4+0551 at $z = 2.79$ which emits very strong and narrow CO(7-6) and [C I] lines (Weiß et al. 2012). The FSM applied to this system yields $\Delta F/F = (6.9 \pm 3.7) \times 10^{-6}$, or neglecting contribution from $\Delta\alpha/\alpha$, we have $\Delta\mu/\mu = -(6.9 \pm 3.7) \times 10^{-6}$ (1σ).

Lensed galaxy HLSJ091828.6+514223 ($z = 5.24$). An upper limit on $\Delta F/F$ was deduced from observation of CO(7-6) and [C I] lines towards the lensed galaxy HLSJ091828.6+514223 at $z = 5.243$ (Levshakov et al. 2012), which corresponds to $\Delta\mu/\mu = (-0.27 \pm 1.53) \times 10^{-5}$ (1σ).

High-redshift [C I]/[C II]/CO systems ($\bar{z} = 6.3$). Two estimates of $\Delta\mu/\mu = (0.0 \pm 2.7) \times 10^{-5}$ at $z = 6.519$ and $\Delta\mu/\mu = (2.3 \pm 3.4) \times 10^{-5}$ at $z = 6.003$ from the previous section can be combined with another high redshift value of $\Delta\mu/\mu = (-1.3 \pm 7.9) \times 10^{-5}$ at $z = 6.419$ towards the quasar J1148+5251 (Levshakov et al. 2017). Being averaged, these three estimates provide a weighted mean value of $\langle\Delta\mu/\mu\rangle = (0.7 \pm 1.2) \times 10^{-5}$ at $\bar{z} = 6.3$ in the epoch of reionization.

The CMB limit on electron mass changes ($z \simeq 1100$). In recent analysis of the cosmic microwave background radiation by Hart & Chluba (2020), it was shown that the electron rest mass, $m_{e,0}$, might be slightly increased during the cosmological recombination era at $z \simeq 1100$: $\Delta m_e/m_{e,0} = (m_{e,z} - m_{e,0})/m_{e,0} = 0.0190 \pm 0.0055$ (1σ).

An important point to note for the CMB analysis is that while only dimensionless numbers are invariant to the adopted system of units, variation of the dimensional parameter m_e for the physics of recombination is equivalent after rescaling to a variation in the dimensionless parameter μ , and “the effect of a variation in m_p on recombination is subdominant compared to a variation in m_e ” (Planck Collaboration et al. 2015). The binding energy of quarks can be also altered but its impact on the atomic and molecular frequencies and on the CMB spectrum is much weaker than the varying electron mass (Kujat & Scherrer 2000; Yoo & Scherrer 2003; Ichikawa et al. 2006).

This paper has been typeset from a $\text{\TeX}/\text{\LaTeX}$ file prepared by the author.

Table A1. Selected H₂ absorption systems from ¹Ubachs et al. 2016, and ²Ubachs et al. 2019.

Quasar	$z(\text{H}_2)$	$\Delta\mu/\mu$ ($\times 10^{-6}$)	$\sigma_{\Delta\mu/\mu}$ ($\times 10^{-6}$)	Refs.
J2123-0050	2.05	-7.6	3.5	1
HE0027-1836	2.40	7.6	10.2	1
Q2348-011	2.43	6.8	27.8	1
Q0405-443	2.59	-7.5	5.3	1
B0642-5038	2.66	-9.44	6.09	2
J1237+064	2.69	4.37	6.30	2
Q0528-250	2.81	0.5	2.7	1
Q0347-383	3.02	-5.1	4.5	1
J1443+2724	4.22	9.5	7.5	1
weighted mean:		-2.5	5.3	